

## GROWTH OF $\text{Al}_2\text{O}_3/\text{Al}$ COMPOSITES FROM Al-Zn ALLOYS

MURALI HANABE<sup>1</sup>, VIKRAM JAYARAM<sup>1</sup> and T. A. BHASKARAN<sup>2</sup>

<sup>1</sup>Department of Metallurgy, Centre for Advanced Study, Indian Institute of Science, Bangalore 560 012 and <sup>2</sup>Materials Science Division, National Aerospace Laboratory, Bangalore 560017, India

(Received 1 September 1994)

**Abstract**—Observations are presented here of the initiation and growth of an  $\text{Al}_2\text{O}_3/\text{Al}$  composite by the directed oxidation of a molten binary Al-Zn alloy with and without preforms. The oxidation behaviour into free space begins with the formation of ZnO on the melt surface followed by a second stage of relatively high growth rate associated with the constant presence of ZnO and a final region of slow growth rate during which the surface consists of both ZnO as well as  $\text{Al}_2\text{O}_3$ . Composite formation is explained on the basis of a cyclic formation and reduction by molten aluminium of ZnO. Oxidation was carried out with ternary Mg additions into  $\text{Al}_2\text{O}_3$  preforms of different particle sizes. The infiltration of an  $\text{Al}_2\text{O}_3$  preform is governed by reaction induced wetting between alloy and ZnO. Nucleation of the alumina is epitaxial with respect to particles of the preform and growth rates are higher than that for composite growth into free space.

### 1. INTRODUCTION

Directed melt oxidation (DIMOX) has emerged as an attractive process to fabricate dense ceramic matrix composites. While this process has been demonstrated to yield matrices of  $\text{Al}_2\text{O}_3/\text{Al}$ ,  $\text{AlN}/\text{Al}$ ,  $\text{Zr}/\text{Zr}$  and  $\text{TiN}/\text{Ti}$ , fundamental research has been directed primarily towards the formation of  $\text{Al}_2\text{O}_3$  based composites from molten Al alloys. Here, the critical role is played by the alloying element in preventing the formation of a protective layer of alumina on the surface of the melt and in promoting the continuous oxidation of Al. Typical alloying additions are Mg, Zn and Si ranging from 0.1 to 10 wt%.

Preliminary studies on DIMOX [1, 2] have emphasized the need for Mg in the alloy if composite growth is to occur and have also indicated the importance of  $\text{MgAl}_2\text{O}_4/\text{MgO}$  surface oxides in controlling the oxygen supply to the underlying Al melt. It is the presence of these non-protective oxides on the surface which leads to the sub-surface growth of alumina. It has also been suggested [3] that a composite can be grown from Al-Si-Zn alloys, only provided the alloy is somewhere in contact with  $\text{MgAl}_2\text{O}_4$ . It was implied that the Zn content in the alloy was necessary only to break the native oxide layer and initiate the growth.

On the other hand, the investigation of the growth of an Al-Mg-Si-Zn-Fe-Cu alloy by Nagelberg *et al.* [4], revealed the presence of a thin ZnO layer on the surface. The composite growth in this case was attributed to the diffusion of ions through the exter-

nal ZnO layer. A recent investigation on this process [5] reports that while Mg is essential to the accelerated growth of the composites, the presence of Si helps in the initiation of the process.

Salas *et al.* [6], suggest that the surface MgO layer in Al-Mg based alloys may result from cation demixing of the thermodynamically stable spinel and thereafter persist in metastable equilibrium with the liquid alloy, thereby preventing the formation of  $\text{Al}_2\text{O}_3$  on the surface. However, they also indicate that the vapour pressure of Mg could be responsible for the continuous presence of MgO on the surface. The presence of the thermodynamically stable spinel prevents the formation of the passivating Al oxide on the surface. On the other hand the role of zinc is less clear in that it is reported to be inactive without the simultaneous presence of Mg but also leads to the formation of surface layers of a thermodynamically unstable oxide.

Investigations in the infiltration of preforms have focused on the microstructure and the associated growth rates [7, 8]. Infiltration of  $\text{Al}_2\text{O}_3$  preforms [7] using an Al-Mg-Si alloy revealed a progressive decrease in the growth rates, that was linked to the build-up of the non-oxidizing element, Si, in the alloy channels. The presence of MgO on the surface suggested a growth mechanism typical of any Al-Mg alloy, but there was no clear indication of the role of the particulate other than the fact that the infiltration rates were higher than those in the absence of a preform. This acceleration in growth rate was also observed for the case of A-380 alloys oxidized into SiC [8] in which it was suggested that the silica layer on the particulate might promote wetting. However,

infiltration of a similar alloy into pre-oxidized SiC [9] occurred at lower growth rates owing to substantial build up of silicon in the alloy channels.

This paper reports the microstructure associated with oxidative growth on binary Al-Zn alloys and of the wetting and infiltration of an inert preform ( $\text{Al}_2\text{O}_3$ ) using an Al-Zn binary alloy, emphasizing the role played by the solute element during the process. Alumina was chosen as the preform material and the alloy used was binary Al-Zn. The criteria for choosing this specific combination stems from the observation that the Al-Zn alloy wetted and climbed the  $\text{Al}_2\text{O}_3$  crucibles during the study of plain composite growth.

In addition, some experiments were carried out on Al-Zn alloys containing 0.3-0.5% Mg, in order to explore the influence of Mg on the uniformity of oxidation. All the alloys used displayed oxidative growth into free space in the presence of a surface layer of ZnO. With Mg contents higher than the ones used here the surface oxide undergoes a transition to a mixture of  $\text{MgO}/\text{MgAl}_2\text{O}_4$  and ZnO [3]. It was decided not to use any Si since preliminary experiments indicated that even small amounts (2-3%) of Si inhibited the infiltration of  $\text{Al}_2\text{O}_3$  compacts, even though other workers have pointed out the beneficial effects of Si in Al-Mg based alloys.

## 2. EXPERIMENTAL PROCEDURE

Aluminium alloys containing 5 and 8 wt% Zn were prepared using high purity Al (99.999) and commercial purity Zn (99.94). Both alloys were melted in an electric resistance furnace and cast into rods of 12 mm diameter. To study the effect of Mg additions on the oxidation behaviour of an Al-Zn alloy, an Al-5Zn-0.3 Mg alloy was also made. The chemical analysis of the cast alloys, as carried out by atomic absorption spectroscopy, is shown in Table 1.

### 2.1. Free space oxidation

The cast rods were machined to fit 8.75 and 9.5 mm i.d. zirconia (CaO stabilized) crucibles. The crucibles were made by cutting a tube to about 12 mm length and sealing the bottom with thin walled  $\text{Al}_2\text{O}_3$  disks using  $\text{Al}_2\text{O}_3$  paste and then firing at  $1500^\circ\text{C}$  for 2 h. Earlier,  $\text{Al}_2\text{O}_3$  crucibles were used for the experiment, but it was observed that the alloy wetted the crucible

considerably and climbed up the crucible walls and oxidized in an uncontrolled manner, thus making weight gain measurements with respect to a particular cross section area impossible. This exaggerated wetting was not observed in the case of  $\text{ZrO}_2$  crucibles and hence the acquisition of reliable data was made possible. Cylinders of height 8 mm were cut from the machined alloy rod using a low speed diamond saw. Just before the experiment the cylinder surface to be exposed was polished on 600 grit SiC paper to remove the native Al oxide. The surface was degreased with methanol and coated with 25-50  $\mu\text{m}$   $\text{Al}_2\text{O}_3$  power of 0.2 mm thickness. This coating ensured that the growth initiated from the entire cross section.

Growth rates were measured by suspending the crucible containing the alloy billet into a high temperature box furnace from the bottom of a balance using a Pt wire. The sensitivity of the balance was 0.01 mg. To shorten the residence time of the alloy at low temperatures and hence minimize the formation of the passivating Al oxide on its surface, the samples were heated rapidly at about  $75^\circ\text{C}/\text{min}$  to  $700^\circ\text{C}$  and beyond to the desired temperature at  $15^\circ\text{C}/\text{min}$ . All the experiments were done in ambient atmosphere. Weight gains were recorded as a function of time at constant temperatures ( $950$ - $1150^\circ\text{C}$ ). The experiments were stopped at different times during the growth to enable characterisation of the surfaces.

### 2.2. Preform infiltration

Preforms of acid washed fused  $\text{Al}_2\text{O}_3$  of  $22\mu\text{m}$  average particle size were prepared with a few drops of PVA as the binder and were pressed to the shape of cylindrical pellets of 10 x 10 mm dimensions. The green preforms were then fired at  $1500^\circ\text{C}$  for 2 h to 40-50% theoretical density to provide mechanical strength for subsequent handling. These 10 mm dia preforms were either used as such in 10 mm i.d.  $\text{Al}_2\text{O}_3$  tubes or machined to fit 7 mm i.d. tubes. The bottom of each tube was sealed as described earlier.

The alloy billet was loosely fitted into the  $\text{Al}_2\text{O}_3$  crucibles to provide for expansion during melting. The coated billet surface in contact with the preform was then loaded into the crucible with the billet at the bottom. The preform fitted tightly into the crucible such that growth was limited to within the preform and did not occur preferentially along the crucible walls. Weight gain was measured as described before or in a high temperature thermobalance (Cahn TG-171).

The grown composites were cut using a low speed diamond saw and cross-sections were polished for optical and scanning electron microscopy. SEM/EDX and Auger spectroscopy were used to study the elemental distribution on the surface. Uninfiltrated regions of the preform were retained and coated with carbon for SEM studies. Specimens were prepared for TEM by dimpling and ion beam thinning.

Table 1. Chemical analysis of alloys

Nominal composition	Analysis	
	Element	Wt%
Al-5 Zn	Zn	4.97
	Mg	<0.00001
Al-8 Zn	Zn	8.47
	Mg	<0.00001
Al-Zn-0.3 Mg	Zn	4.97
	Mg	0.36

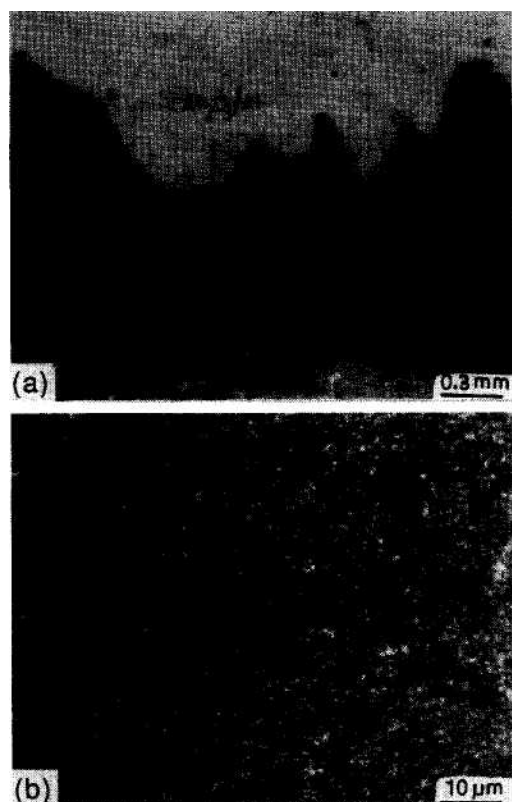


Fig. 1. Cross-section of the composite grown from an Al-Zn alloy. Part (a) is the lower magnification view showing undulations on the surface; (b) is the higher magnification picture showing  $\text{Al}_2\text{O}_3$  and metal.

### 3. RESULTS

Figure 1 shows the cross-section of the composite grown by oxidizing an Al-5 wt% Zn alloy. The small bright dots are the metal channels of the order of 0.1-0.5  $\mu\text{m}$ . The dark background is  $\text{Al}_2\text{O}_3$  which comes from the oxidation of the Al. The volume fraction of the metal was measured by analysing a SEM image of the cross-section and is estimated to be between 10 and 15%.

Figure 2(a) shows TGA plots for an Al-5 wt% Zn alloy at different temperatures. Though the growth rates vary with temperature the shape of the curves and the oxidation behaviour remain essentially the same. The curves basically exhibit three stages during the process. There is a slow initial weight gain followed by a second stage of increasing growth rate. The thickness of composite grown during this second stage increases with zinc content but shows substantial variability with respect to temperature in the range studied.

Figure 2(b) shows that the growth rate of composite increases in going from 5 to 8 wt% Zn at 1050°C (alloys with 1% Zn did not display any growth at all). It is also seen that, while the composite growing from Al-5 wt% Zn has tailed off, the composite growing from an Al-8 wt% Zn is still in the high growth stage. Different samples may exhibit

different initiation times but once the process starts the same oxidation behaviour is followed. Since the microstructural evolution follows the same pattern at different temperatures the succeeding paragraphs will therefore describe the morphology of growth at different stages only for the composite grown at 1050°C.

In the initial stage of the growth process, corresponding to a weight gain of about 5-15  $\text{mg cm}^{-2}$ , the melt develops a light grey coloured oxide gradually over the entire cross section, as seen in Fig. 3(a). The SEM image [Fig. 3(b)] shows the oxide to be porous and having a feathery morphology similar to that shown in Ref. [3], while EDX analysis using SEM on this region identified only Zn, suggesting that this oxide is ZnO.

In the second stage the ZnO layer thickens and subsequently remains more or less constant at 2-5  $\mu\text{m}$ . Figure 4 shows typical X-ray maps of Al and Zn of the cross-section of the composite near the surface during this stage. In the Al X-ray map the brighter regions correspond to metal channels surrounded by  $\text{Al}_2\text{O}_3$ . It is evident that ZnO is present only at the surface and superimposition of the two

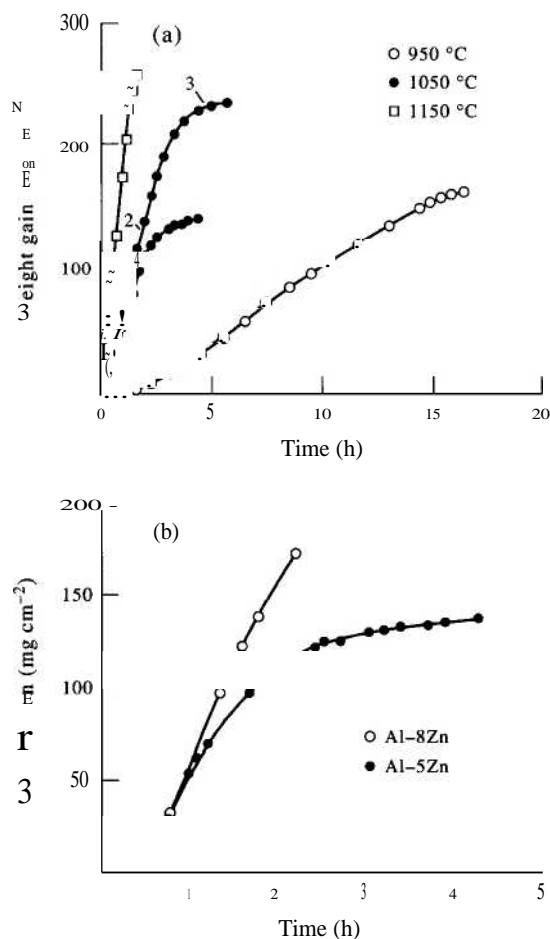


Fig. 2. (a) TG plots for an Al-5Zn alloy at different temperatures. (b) TGA of Al-5Zn and Al-8Zn alloys at 1050°C.

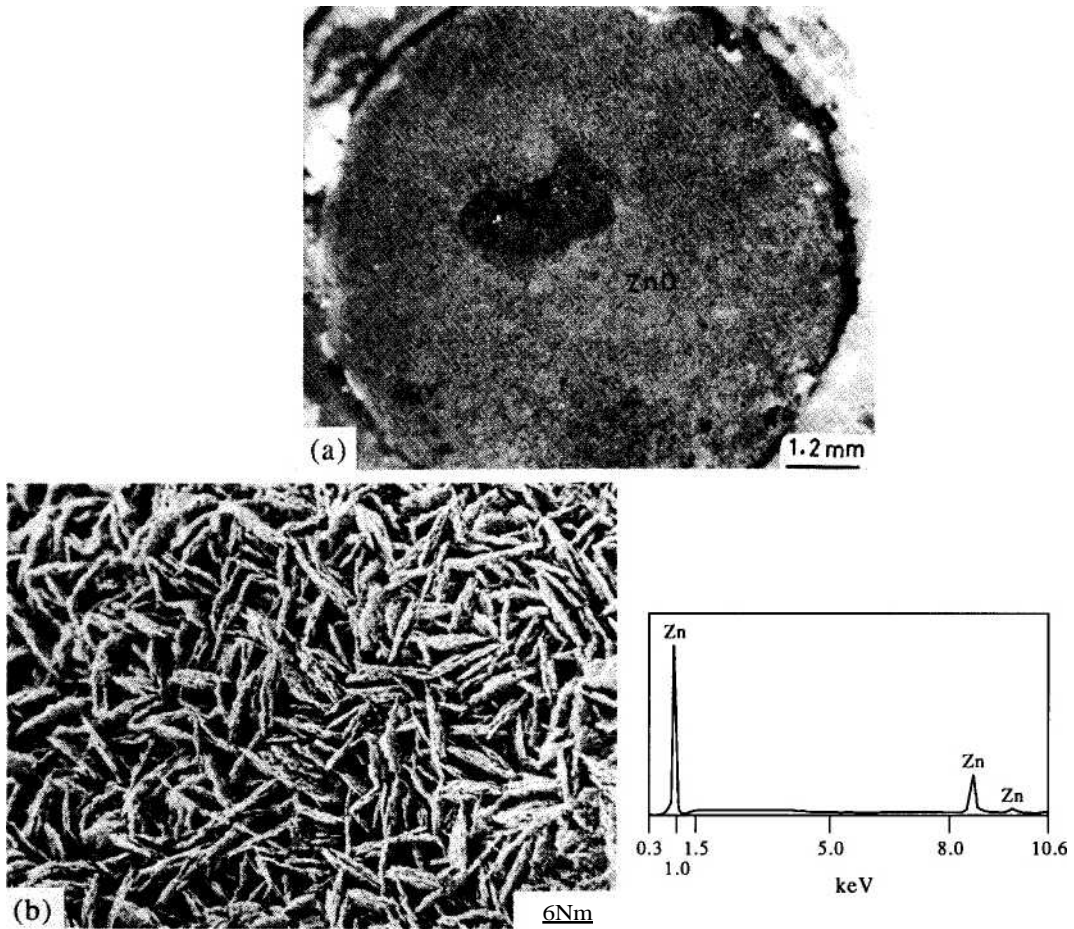


Fig. 3. Surface of the composite in the initial stage of the growth. Part (a) is the low magnification micrograph; (b) is the SEM image of the region showing porous ZnO and the corresponding EDAX spectrum.

X-ray maps shows that there is frequently a metal layer between the surface ZnO and the underlying  $\text{Al}_2\text{O}_3$ .

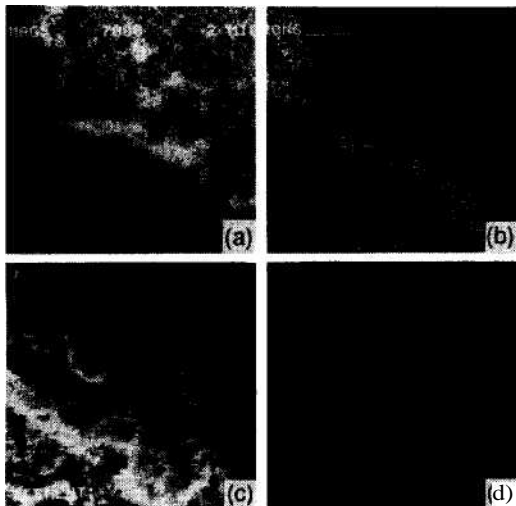


Fig. 4. X-ray maps of the cross-section of the composite showing Al in contact with the surface ZnO.

The oxidation rate decreases as growth approaches the third stage while the surface morphology becomes less uniform with respect to ZnO distribution and develops undulations in the form of ripples. Figure 5, which shows the boundary between the peaks and the valleys, indicates that the circumference of the ripple has the feathery ZnO structure while the centre displays a fine nodular morphology. X-ray analysis reveals that Zn is present in both regions though predominantly in the peaks, while Al is more concentrated in the valleys. Energy dispersive X-ray analysis of the aluminium rich region reveals an average Al content of 85-90 at.%.

Auger spectroscopy was carried out on nodular regions revealing three types of elemental distribution as illustrated in Fig. 6. The feathery morphology is now completely absent even in those parts that show predominantly Zn. It is clear that there exist portions of the surface that are devoid of zinc and that the composition of the oxide at the end of stage 2 has begun to fluctuate between pure ZnO and  $\text{Al}_2\text{O}_3$ , even in regions as small as 0.1  $\mu\text{m}$  (the electron probe diameter). More precise quantitative correlations could not be made owing to the rough surface

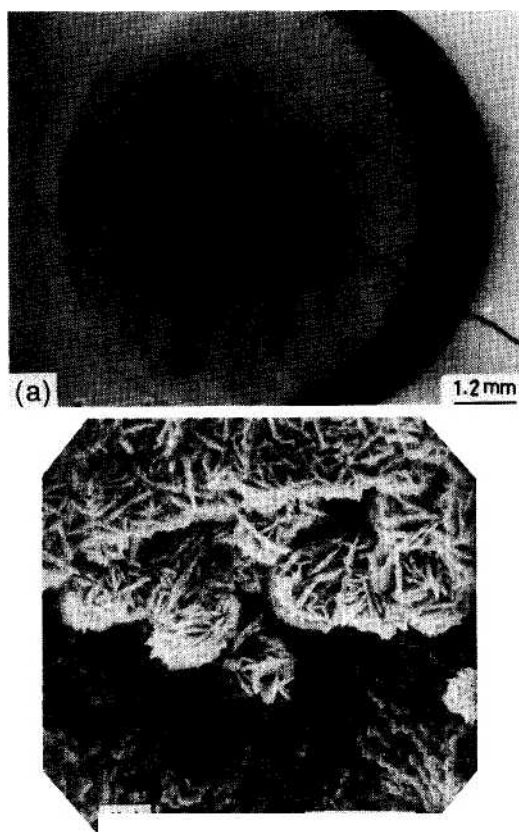


Fig. 5. Surface of the composite during stage 2-3 transition. Part (a) shows the development of undulations on surface; (b) is the SEM image of a region showing both centre and circumference of a ripple.

topography. But it may be noted that regions which display strong Al signals indicate both elemental as well as ionized species. Thus, alloy channels are probably present to within the depth resolution of Augers spectroscopy, i.e. 20Å below the surface. Comparison of peak height ratios with sintered standards suggest non-stoichiometric ZnO with a Zn/O ratio > 1.

In the third stage of the growth curve, the surface ripples have amplified as shown in Fig. 7(a). Closer examination shows large flat pockets on the maxima that reveal only an Al signal as seen in Fig. 7(b), thus suggesting that these flat regions are  $\text{Al}_2\text{O}_3$ . On the other hand a spectrum from the minima between ripples which possess a fine nodular structure similar to that which was seen during the second stage of the process, shows a mixed Al and Zn signal. The major contribution to the weight gain now appears to be derived from these isolated regions of nodular growth within the troughs.

### 3.1. Oxidation into alumina preforms

The oxidation behaviour of the magnesium containing alloy displays a longer duration of stage 2 growth region compared to that in the case of the binary Al-Zn alloy. However, X-ray analysis in the

SEM on this surface detected only Zn and Al signals in the ratio Zn:Al of 80:20 at. %.

Figure 8 shows the optical micrograph of the cross-section of the composite and TGA curves for the composites grown from Al-Zn-Mg into free space and infiltrated through a preform of 23µm particulate at 1050°C, respectively. The process starts slowly, as a planar front develops across the entire surface after which the rate is 2-4 times higher than for growth into free space. Furthermore, the rapid reduction in growth rate that is displayed in free space is not observed here. Metal channel dimensions are ~0.3 µm and are comparable to those obtained in the absence of a preforma.

After every experiment the inner walls of the crucible above the infiltrated preform had a coating of a white powder which was identified as ZnO by X-ray diffraction. Scanning electron microscopy of uninfiltrated regions of the preform revealed crystallites on top of the particles of the  $\text{Al}_2\text{O}_3$  preform as shown in Fig. 9(a). X-ray analysis of these particles [Fig. 9(b)] revealed a Zn signal thus confirming the presence of ZnO. It was possible to interrupt an experiment to examine in sections, a partially infiltrated portion of composite. The overall view of alumina particulate with metal in-between is shown in Fig. 10(a). A closer view Fig. 10(b), shows the beginnings of a composite layer growing outwards from the particle surface.

The most significant finding in the TEM, illustrated in the dark field image in Fig. 11(a), is the similarity

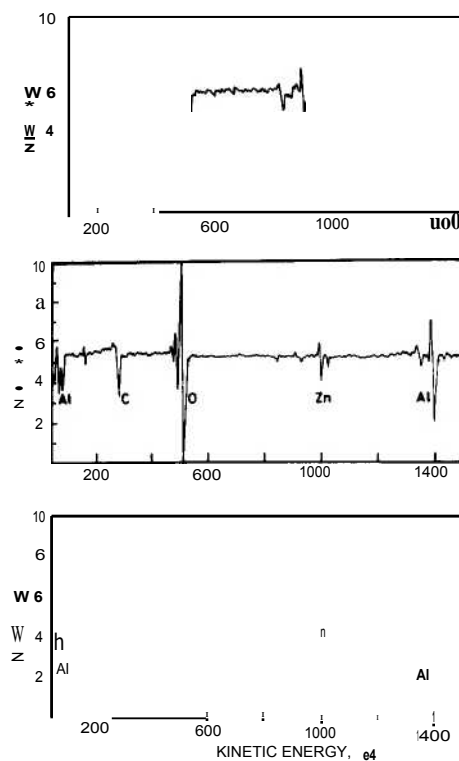


Fig. 6. Auger spectra of nodular regions.

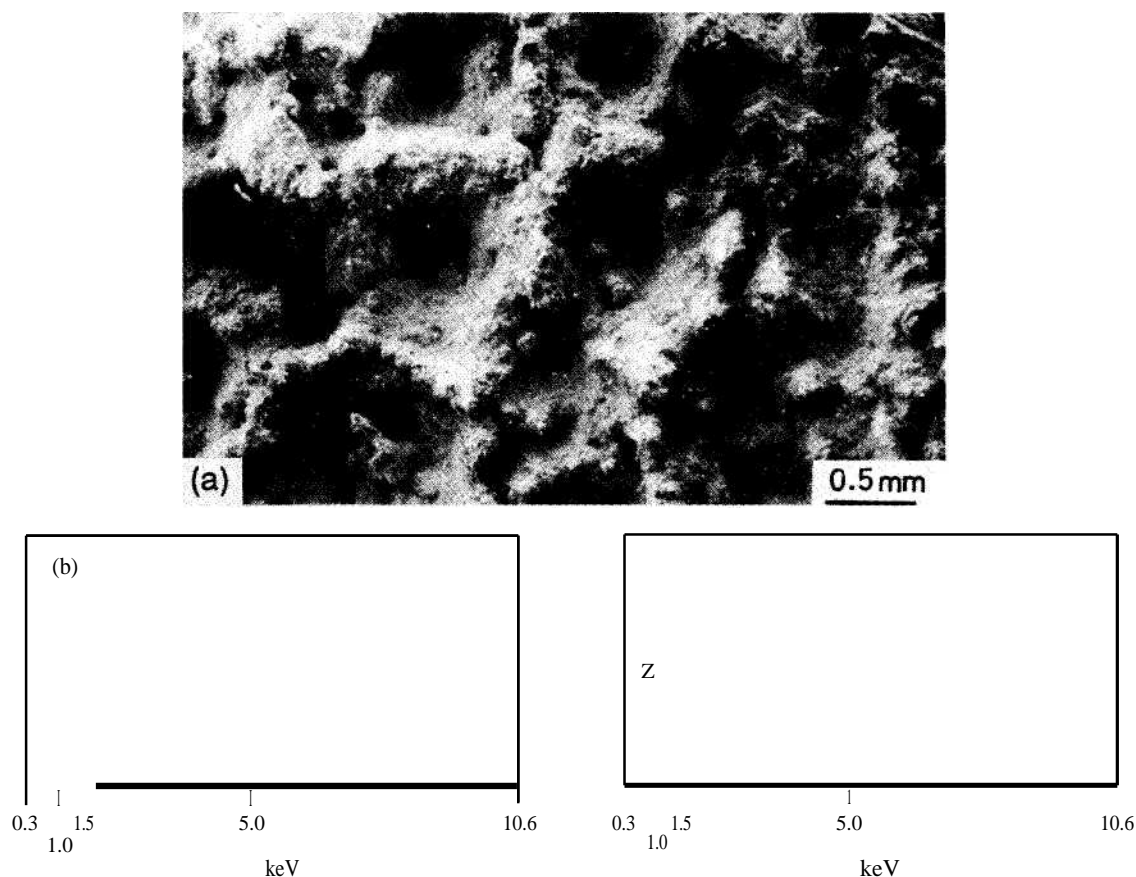


Fig. 7. Surface during stage 3. (a) SEM image showing the well defined peaks and troughs on the surface. (b), (c) EDAX spectra showing the presence of  $\text{Al}_2\text{O}_3$  on top of the peaks in (a) and the presence of both  $\text{ZnO}$  and  $\text{Al}_2\text{O}_3$  in the valleys, respectively.

in orientation between the preform particle and the oxidation product. Typically, the orientation extends out to 2–5  $\mu\text{m}$  away from the particle surface before it meets another  $\text{Al}_2\text{O}_3$  crystal that is growing out from yet another particle. This epitaxy is maintained quite faithfully everywhere on the particle surface as illustrated by the  $\sim 1 \mu\text{m}$  region [Fig. 11(b)] where the preform particle displays a twin whose orientation is exactly duplicated in the adjacent oxidation product. Further details of the microstructure are shown in Figs 12 and 13. A dark field image taken with an Al reflection reveals that the major portion of the metal film lies between two layers of oxidation product that have formed on two preform particles. However, one observes frequently at the particle-matrix interface, a row of 10–50 nm circular regions which also appear bright in the same dark field image [Fig. 12(b)], suggesting that they are remnants of a metal film. Similarly, the dark field-bright field pair (Fig. 13), where the  $\text{Al}_2\text{O}_3$  is strongly diffracting, reveals, from the discontinuity in the bend contour, the presence of  $\sim 15 \text{ nm}$  interfacial layer, probably metal.

Figure 14(a) shows the time dependence of weight gain for different particle sizes that were infiltrated using Al-Zn-Mg. The rates were normalized to the actual porosity as measured by the weight and vol-

ume of the preform. While all preforms are infiltrated faster than growth occurs on an open melt the trend is not monotonic with particle size.

#### 4. DISCUSSION

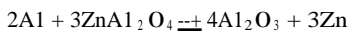
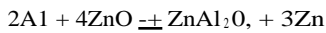
##### 4.1. Oxidation

The limited literature on the low temperature oxidation of Al-Zn alloys does not clearly identify the surface oxide. Scamans *et al.* [10], have suggested that the addition of Zn to Al delays the nucleation of  $\gamma\text{-Al}_2\text{O}_3$  crystals and promotes pore formation in the oxide. They have also indicated that the expansion of the  $\gamma\text{-Al}_2\text{O}_3$  lattice may be due to the inclusion of Zn ions and the formation of  $\text{ZnAl}_2\text{O}_4$ .

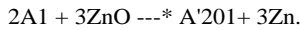
Thus it can be assumed that the Zn comes to the surface subsequent to the formation of the native Al oxide. It has been stated [3] that the presence of Zn may help in the rupture of the native oxide and start the growth due to the high vapour pressure of Zn. The vapour pressure of Zn over an Al-5 wt% Zn alloy at the temperatures involved in this study is  $\sim 0.1$  atmosphere at  $1100^\circ\text{C}$  if ideal behaviour is assumed. It is therefore unlikely that bulk rupture of the oxide film can occur. However, as pointed out earlier [10], the presence of pores in the oxide layer or cracking during melting could be a means of escape

for the Zn vapour to escape and oxidize. While the presence of MgO on the surface in Al-Mg alloys has been attributed to both, demixing of MgAl<sub>2</sub>O, as well as to the vapour pressure of Mg, the ZnO on the surface of the composite and on the crucible walls can come about only by the vapour phase oxidation of Zn.

The high growth rate regime in the weight gain-time curves is associated with the constant presence of ZnO on the surface. Cross-sections of the composite revealed that the surface ZnO is in contact with the metal and that the Al<sub>2</sub>O<sub>3</sub> is separated from the ZnO by a metal layer. Two types of reactions involving the liquid Al and ZnO can be envisaged. Both involve a final reduction of ZnO to elemental zinc but in one case an intermediate spinel is formed



or



It is possible to show that both the spinel as well as ZnO are in equilibrium with alloys of practically pure zinc, i.e. both oxides are extremely metastable with respect to alumina when in contact with

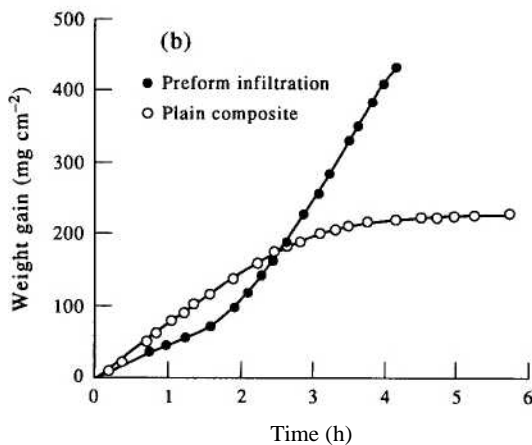
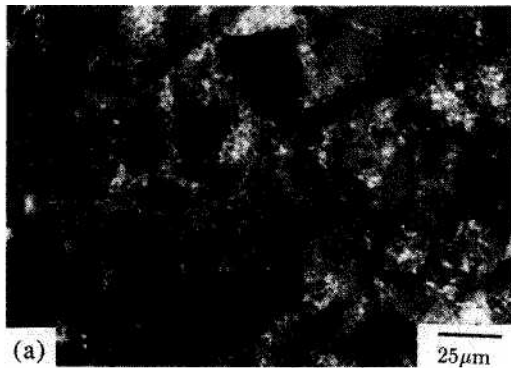


Fig. 8. (a) Optical micrograph of alumina particulate infiltrated with Al<sub>2</sub>O<sub>3</sub>/Al composite (Al-5Zn, 1050°C). (b) Weight gain normalized comparison between oxidation into free space and into particulate.

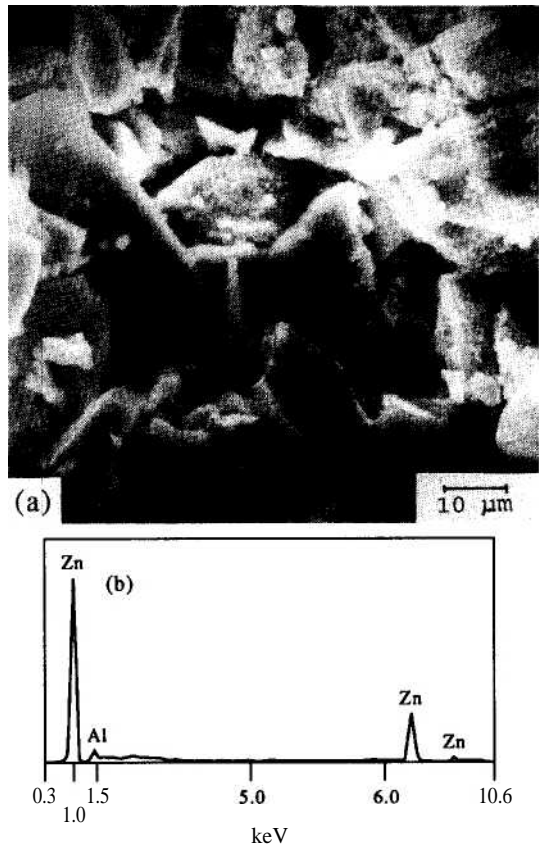


Fig. 9. Uninfiltrated portion of preform with coating of Zn rich particles (a) whose X-ray spectrum is shown in (b).

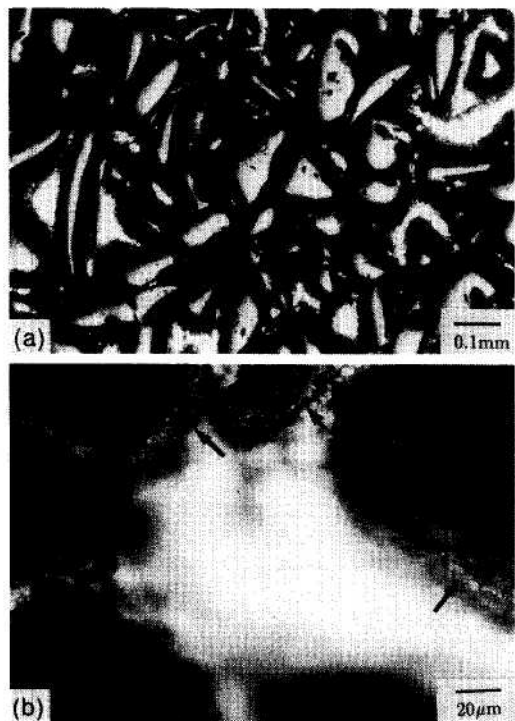


Fig. 10. Optical micrograph showing bright metal channels between particles (a) and a thin layer of oxidation product on the surfaces of particles (b).

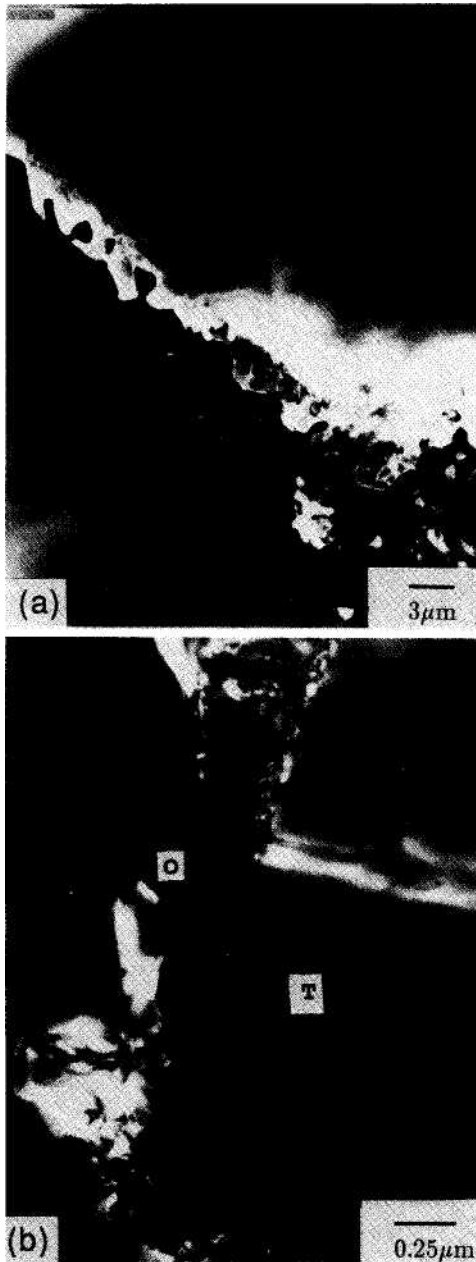


Fig. 11. (a) Dark field electron micrograph using a preform reflection indicating the overall similarity in orientation between the particle and the oxidation product. In (b), a twin of  $-0.5$  pm width in the particle, T is reproduced in the oxidation product, o.

molten alloy of 5% Zn. Thus, the interfacial reaction appears as a likely candidate for the mechanism by which alumina is formed. As with the case of Al-Mg based alloys [5, 6] the alumina forms by dissolution of oxygen at the Al-ZnO interface and by re-attachment after reaction at the underlying Al- $\text{Al}_2\text{O}_3$  interface. Such a step obviates the need for re-nucleation of alumina on zinc oxide. This mechanism is proposed as an alternative to an earlier study [4] in which it was suggested that the ZnO layer on the surface con-

tributed to the growth of the composite by providing a path for diffusion of the ionic species.

A pre-requisite for the growth of the composite is the manner in which the liquid metal supply is maintained to the reaction front. Diffusion couples between (Al, Zn) and sintered ZnO carried out as part of the present work showed that the reaction product of alumina does not form a continuous layer but that the alloy wets the interface between ZnO and the  $\text{Al}_2\text{O}_3$ , similar to the microstructure during composite growth (Fig. 4). This wetting phenomenon is therefore a likely source of metal channels.

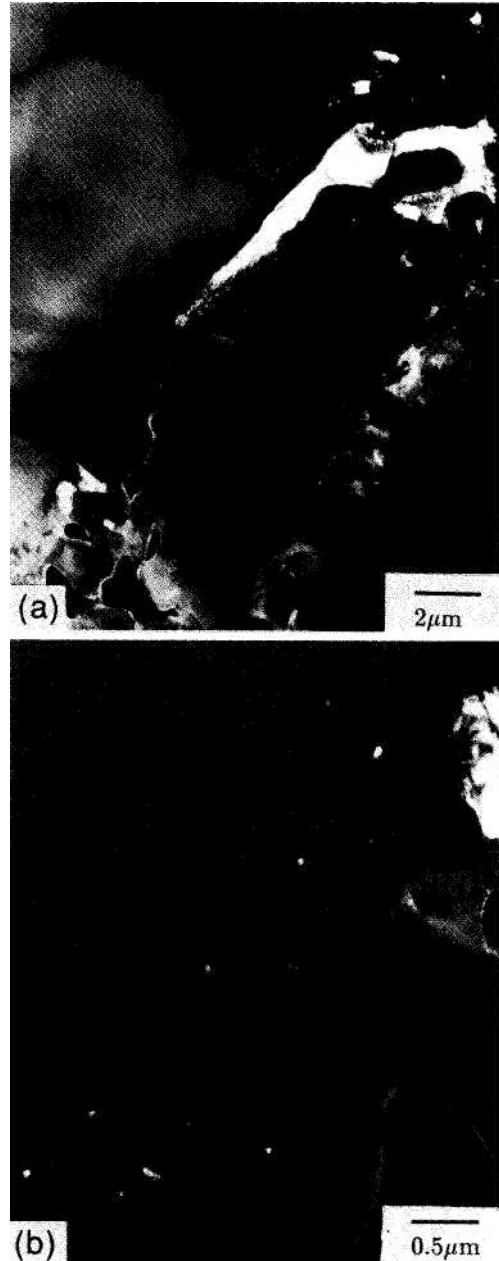


Fig. 12. Dark field taken with an Al reflection showing the penetration of metal between two particles (a). A higher magnification of the interface in (b) between the particle and the oxidation product shows small bright pockets of metal.



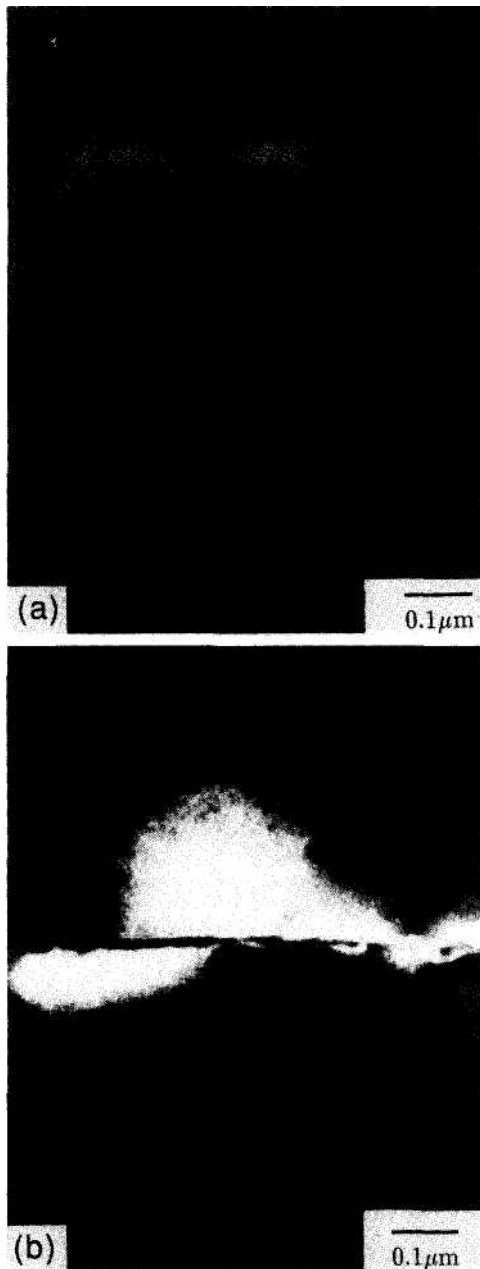


Fig. 13. Bright field (a) dark field (b) pair with alumina under strong dynamical conditions (bottom = preform, top = oxidation product) showing the presence of an interfacial layer.

As the third stage in the growth curve is approached, the surface microstructure was observed to develop undulations. Some regions on the surface showed lower concentrations of Zn, as reflected by the absence of the feathery ZnO structure. A similar instability in growth has been observed during the oxidation of Al-Mg-Si alloys [11, 12]. Composite growth was observed to occur in a steady state fashion initially, but after a certain time the composite developed a banded structure with varying  $\text{Al}_2\text{O}_3$  to metal volume fraction. The oscillations in

the growth rate were associated with the fluctuations in the Mg concentrations in the alloy near the surface.

A clear explanation for the drop in growth rate in stage 3 in the present study is not presently available. However, one may note the following points. There is no significant change in either the distribution of the alloy channels or in the Zn content of the bulk alloy at the onset of the decrease in growth rate. Thus, one may tentatively exclude, as causes for the passivation, a reduction in the bulk availability of Zn. However, diffusional limitations through the tortuous sub-micron alloy channels could conceivably limit the concentration of zinc at the composite surface. Thus, the sub-surface reaction to form  $\text{Al}_2\text{O}_3$  now extends to the surface thereby blocking metal channels. The increase with Zn content in the magnitude and duration of the regime of high growth follows as a consequence of such a hypothesis. The re-initiation of growth within the troughs of the microstructure [Fig. 5(a)] represent a process akin to the incubation period that precedes stage 1 wherein the native  $\text{Al}_2\text{O}_3$  layer must be re-penetrated by alloy channels.

The role of Mg, it must be stated at the outset, is dependent on the relative amounts of Mg and Zn and also on the presence of other elements, notably Si. It is worth comparing the composition of the surface oxide in the present and other experiments. Al-5Zn-0.3Mg yields an oxide containing predominantly Zn with some Al, Al-3Zn-3Si-0.5Mg yields MgO [12], Al-12.5Zn-0.1Mg-4.5Si yields MgO and ZnO [3], while Al-8.8Si-2.8Zn-0.25Mg-3.1Cu-1.1Fe yields only ZnO. The presence of Mg in quantities large enough to yield MgO involves a change in the mechanism of DIMOX and the present work suggests the following explanation of the superior role of Al-Zn-Mg compared to Al-Zn, namely, when vaporization is not adequate due to local surface depletion of solute and the thermodynamically stable oxide

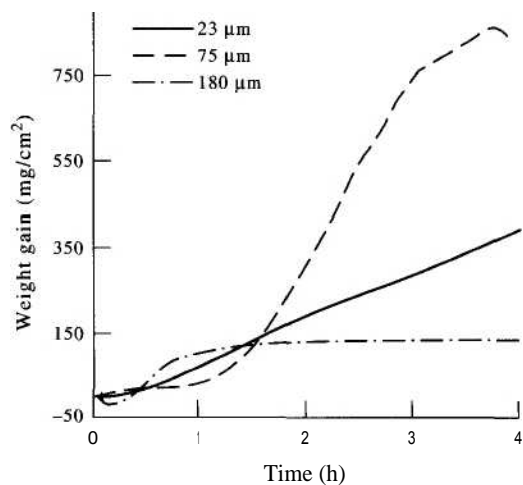


Fig. 14. Normalized weight gain as a function of particle size (Al-5Zn-0.3Mg, 950°C). The deviation after 750  $\text{mg cm}^{-2}$  for 75  $\mu\text{m}$  is due to the composite growing out of the preform.

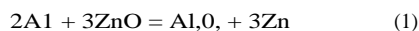
forms on the surface,  $\text{MgAl}_2\text{O}$ , is less passivating than  $\text{Al}_2\text{O}_3$ . Consequently, re-penetration of any local blockage is far more readily carried out in Al-Mg than in Al-Zn based alloys, where the nomenclature refers to the oxide of the appropriate solute that is present on the surface of the composite.

#### 4.2. Infiltration

The most striking feature observed during the infiltration of preforms was the epitaxy between the preform and the oxidation product, which unquestionably supports the hypothesis that nucleation of the oxide begins predominantly on the surface of the particulate. This is in sharp distinction to the approximately monocrystalline orientation over hundreds of microns that has been reported for the case of oxidation into free space [1, 6].

In a reactive system the free energy changes associated with wetting are linked to the changes in mass of the various phases [14]. Mass transfer occurs across the interface leading to a decrease in the specific free energy of the system,  $g_s'$  by chemical reaction where  $g_s' = GS'/A$ , where  $G'$  is the free energy change at the interfacial region.

For the equilibrium reaction



$G^\circ = -648$  kJ/mol at 1300 K using thermodynamic data obtained from standard tables [15].

If  $a_{\text{Zn}} = 0.02$ ;  $a_{\text{Al}_2\text{O}_3} = 0.98$ , assuming ideality in liquid.  $G = -773$  kJ/mol.

If  $t$  is the effective thickness of the ZnO layer and if it is assumed that all the ZnO in this volume is replaced by  $\text{Al}_2\text{O}_3$  due to reaction 1, then the change in the specific interfacial free energy is

$$\Delta g_s^A = \frac{G}{3} \times \frac{t \text{ZnO} \rho_{\text{ZnO}}}{M_{\text{ZnO}}} \\ = 17.8 \times 10^3 t \text{ J m}^{-2} \quad (2)$$

where  $t$ ,  $P$  and  $M$  are the thickness, density and molecular weight respectively of ZnO.

For a film of  $0.1 \mu\text{m}$ , this negative change of  $-18 \text{ J m}^{-2}$  in the interfacial free energy is one order of magnitude greater than typical surface/interfacial energies and will contribute to the spreading of the liquid alloy between the ZnO layer and the preform particle, suggesting that significant driving force for supply of liquid metal to the  $\text{Al}_2\text{O}_3$  surface can be provided by the chemical reaction.

The phenomenon of reaction induced wetting is sensitive to the substrate as well as the alloy composition. For example,  $\text{ZrO}_2$  crucibles did not display the extensive and adherent ZnO film that was ubiquitous on  $\text{Al}_2\text{O}_3$  crucibles. Correspondingly, Al-Zn alloys could not be used to infiltrate  $\text{ZrO}_2$  powder preforms. On the other hand  $\text{Si}_3\text{N}_4$  was readily infiltrated.

It has been reported that Al-Mg-Si alloys display accelerated growth into  $\text{Al}_2\text{O}_3$  preforms [7] but that the oxidation product displays no epitaxy with the

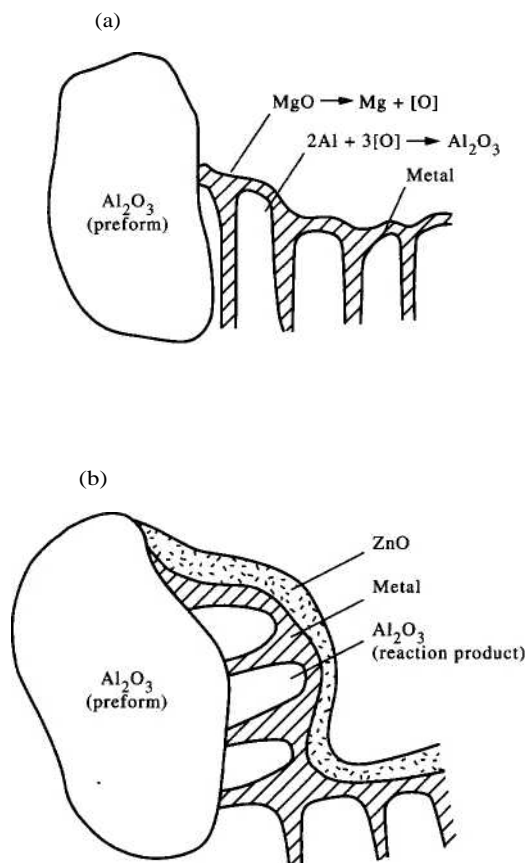


Fig. 15. Schematic illustrating two possible microstructural mechanisms for infiltration in the case of a surface MgO layer (a) and a surface ZnO layer, (b).

particles of the preform. It was also not reported whether MgO coatings were found on the particle surfaces. But it was observed that the interface between preform and oxidation product did not display any layer of alloys. These two microstructures are schematically shown in Fig. 15 (a and b). Epitaxial growth takes place on whichever substrate is adjacent to the alloy. Since the ZnO-preform interface is wet by the alloy, growth takes place from the particle surface. In the absence of such setting, as is presumably the case with the MgO-preform interface, while the preform continues to provide additional surface area for oxidation the orientation of the oxidation product follows that of the "matrix", i.e. with [0001] lying along the local growth direction which, in a powder compact can deviate substantially from the global growth direction. Thus, macroscopically the growth texture would be eliminated in the first case (ZnO) and greatly reduced in the second (MgO).

Since the pore volume in the experiments varied with particle size it is not intended to attempt to fit the data in Fig. 14 to a theoretical model. However, two features clearly stand out. The first is that, as expected, we recover the oxidation behaviour in the absence of a preform when the particle size (pore size)

is large; in this case 180  $\mu m$ . The rapid initial transient leading to a deceleration and greatly reduced growth rate is characteristic of oxidative growth into free space of high zinc alloys (even Mg in trace amounts). Finer particulate are able to sustain steady state growth indefinitely (up to 5 mm).

Secondly, the growth rate is higher for 75 nm than for the finest particles of 23  $\mu m$ . It is tentatively suggested that the reason for this is that the height of the zinc oxide layer is not a constant, but drops with the particle size as the ability of the vapour to migrate diminishes owing to the increased surface area available for nucleation and the increased tortuosity of the pore channels. However, more systematic study is needed to ascertain the influence of pore size.

### 5. CONCLUSIONS

1. Initial oxidation rates of binary Al-Zn following the appearance of a feathery surface layer of ZnO are high.  $Al_2O_3$  formation occurs by a cyclic process of oxidation of Zn vapour followed by an exchange reaction between Al and ZnO. Subsequently, the oxidation rate falls as the concentration of ZnO decreases on the surface. The morphology of the oxide becomes more nodular and growth of composite is restricted to Zn rich regions that develop as perturbations. Eventually, even these protuberances become static while fresh nodules nucleate further down in the troughs.

2. The duration and magnitude of steady state growth increases with increasing Zn, temperature and minor additions of Mg.

3. Al-Zn alloys can be used to infiltrate A1203 preforms at rates that are up to four times the maximum achieved into free space at 950-1050°C. This high infiltration rate can be sustained in a preform with particles below a critical size, in contrast to the rapid decay in growth observed in very coarse particulate or into free space.

4. The volatility of Zn plays a major role in

the wetting and growth of the composite within the preform. A coating of ZnO on the particle surface ahead of the main growth front controls the supply of liquid metal to the particle surface by a process of reaction induced wetting. The orientation of the oxidation product follows that of the substrate particle upon which nucleation occurs.

*Acknowledgements*-The authors would like to thank Joyce Olsen of the Materials Department, University of California at Santa Barbara for carrying out Auger Spectroscopy and the Materials Department at the University of California-Santa Barbara for making available the Scanning Auger Microprobe.

### REFERENCES

1. M. S. Newkirk, A. W. Urquart, R. Zwicker and E. Breval, *J. Mater. Res.* 1, 81 (1986).
2. S. Antolin, A. S. Nagelberg and D. K. Creber, *J. Am. Ceram. Soc.* 75, 447 (1992).
3. M. Sindel, N. A. Travitzky and N. Claussen, *J. Am. Ceram. Soc.* 73, 2615 (1990).
4. A. S. Nagelberg, *Solid St. Ion.* 32/33, 783 (1989).
5. A. S. Nagelberg, *J. Mater. Res.* 7, 265 (1992).
6. O. Salas, H. Ni, V. Jayaram, K. C. Vlach, C. G. Levi and R. Mehrabian, *J. Mater. Res.* 6, 64 (1991).
7. A. S. Nagelberg, *Proc. Mater. Res. Soc.* 155, 275 (1989).
8. E. Manor, H. Ni, C. G. Levi and R. Mehrabian, *J. Am. Ceram. Soc.* 73, 2615 (1990).
9. S. P. Dhandapani, V. Jayaram and M. K. Surappa, *Acta metall. mater.* 42, 649 (1994).
10. G. M. Seamans and E. P. Butler, *Metall. Trans.* 6A, 2055 (1975).
11. K. C. Vlach, O. Salas, H. Ni, V. Jayaram, C. G. Levi and R. Mehrabian, *J. Mater. Res.* 6, 1982 (1991).
12. O. Salas, V. Jayaram, K. C. Vlach, C. G. Levi and R. Mehrabian, in *Banded Microstructures in  $Al_2O_3/Al$  Composites Produced by Oxidation of Molten Al-Mg Alloys*. The Minerals, Metals and Materials Society, Conference on Processing and Fabrication of Advanced Materials for High Temperature Materials (1992).
13. V. Jayaram, unpublished work.
14. I. A. Aksay, C. E. Hoge and J. A. Pask, *J. Phys. Chem.* 78, 1178 (1974).
15. P. Bolsaitis and P. M. Sullivan, *Trans. TMS-AIME* 245, 1435 (1969).